

## ***Dictyostelium* myosin I<sub>K</sub> is involved in the maintenance of cortical tension and affects motility and phagocytosis**

**Eva C. Schwarz, Eva M. Neuhaus, Claudia Kistler, Andreas W. Henkel and Thierry Soldati\***

Department of Molecular Cell Research, Max-Planck-Institute for Medical Research, Jahnstrasse 29, D-69120 Heidelberg, Germany

\*Author for correspondence (e-mail: soldati@mzf.mpimf-heidelberg.mpg.de)

Accepted 2 December 1999; published on WWW 31 January 2000

### **SUMMARY**

*Dictyostelium discoideum* myosin I<sub>K</sub> (MyoK) is a novel type of myosin distinguished by a remarkable architecture. MyoK is related to class I myosins but lacks a cargo-binding tail domain and carries an insertion in a surface loop suggested to modulate motor velocity. This insertion shows similarity to a secondary actin-binding site present in the tail of some class I myosins, and indeed a GST-loop construct binds actin. Probably as a consequence, binding of MyoK to actin was not only ATP- but also salt-dependent. Moreover, as both binding sites reside within its motor domain and carry potential sites of regulation, MyoK might represent a new form of actin crosslinker. MyoK was distributed in the cytoplasm with a significant enrichment in dynamic regions of the cortex. Absence of

MyoK resulted in a drop of cortical tension whereas overexpression led to significantly increased tension. Absence and overexpression of MyoK dramatically affected the cortical actin cytoskeleton and resulted in reduced initial rates of phagocytosis. Cells lacking MyoK showed excessive ruffling, mostly in the form of large lamellipodia, accompanied by a thicker basal actin cortex. At early stages of development, aggregation of *myoK* null cells was slowed due to reduced motility. Altogether, the data indicate a distinctive role for MyoK in the maintenance and dynamics of the cell cortex.

Key words: *Dictyostelium discoideum*, Myosin, Actin cortex, Motility, Phagocytosis, Cortical tension

### **INTRODUCTION**

The myosins are a very rapidly expanding protein family subdivided into at least 15 structural and phylogenetic classes (Mermall et al., 1998; Probst et al., 1998; Wang et al., 1998). Accordingly, the traditional definition of a myosin as a motor protein that translocates along actin filaments in an ATP-dependent manner is likely to be too restrictive to account for the wide spectrum of tasks that myosins support within the cell. Myosins function in a multitude of cellular processes such as motility, cytokinesis, phagocytosis, endocytosis, polarized secretion and exocytosis, organelle movement and mRNA transport (Mermall et al., 1998). Aside from the ubiquitous myosin IIs, myosins of class I are the most heterogeneous class and are among the most abundant in the cell. Some class I myosins have been extensively characterized biochemically over the last 20 years (Hammer et al., 1983, 1984; Pollard and Korn, 1973), but relatively little is known about their precise cellular and molecular functions.

The mechanisms of motor activity are well understood for the classical myosin II (Sellers and Goodson, 1995), and for some myosins of class I (Hayden et al., 1990; Ostap and Pollard, 1996a). As a consequence, the structure/function analysis of myosins is based on the general principles arising from the study of the paradigm myosin II. Myosins consist of three domains, and the crystal structure of the motor domain

of myosin II has been solved (Rayment et al., 1993). Within this highly conserved domain, two flexible surface loops have been observed that vary both in length and sequence. Loop1 is localized near the ATP-binding pocket (Spudich, 1994) and was recently shown to tune the rate of ADP release (Murphy and Spudich, 1998; Rosenfeld et al., 1998), thereby controlling velocity. Loop2 is positioned at the actin binding site and interacts with the negatively charged amino-terminal part of actin (Furch et al., 1998) and appears to modulate the actin-activated ATPase activity.

Structurally, the second domain, called the neck, is an  $\alpha$ -helix thought to act as a lever arm (Uyeda et al., 1996). It is stabilized by the binding of light chains, proteins of the calmodulin/EF-hand family (Sellers and Goodson, 1995), to a consensus binding peptide containing the IQ motif (Rhoads and Friedberg, 1997).

The third domain or tail is the most variable part of the molecule and has classically been defined restrictively as the cargo-binding domain. It has been suggested to reflect the adaptation of myosins to extremely diverse and class-specific functions (Mermall et al., 1998). In most class I myosins, the tail is composed of three subdomains: a basic phospholipid binding domain (Adams and Pollard, 1989; Miyata et al., 1989); a second domain called GPA or GPQ for its high content in Gly, Pro and either Ala or Gln, shown in vitro to contain a secondary ATP-independent actin-binding site (Jung and

Hammer, 1994; Rosenfeld and Renner, 1994); and finally an SH3 (Src homology 3) domain (Mayer, 1997).

We study actin and myosin function in the biochemically and genetically tractable eukaryotic model organism *Dictyostelium discoideum*, which is an intermediate in complexity between *S. cerevisiae* and *H. sapiens*. *D. discoideum* expresses seven class I myosins (Uyeda and Titus, 1997; Schwarz et al., 1999). As the deletion of single myosin I genes resulted in only subtle phenotypes, most functional data were derived from myosin double or triple knock-out mutants. Mutant strains oversecrete lysosomal enzymes and show defects in pseudopod extensions, fluid phase endocytosis, streaming and terminal development (Jung and Hammer, 1990; Temesvari et al., 1996; Wessels et al., 1996).

In the present study, we report the characterization of a novel type of myosin related to class I myosins but containing unique structural features, including an oversized loop1 and the virtual absence of neck/tail domain. We present evidence that MyoK may act as an actin cross-linker that can be regulated. Loop1 was shown in vitro to contain a salt-sensitive secondary actin-binding site. Despite these unusual features, *D. discoideum* MyoK binds actin in an ATP-dependent fashion. In order to study the function of MyoK in vivo, we analysed the phenotypic alterations in *myoK* null cells (*myoK*<sup>-</sup>) and MyoK overexpressing cells (MyoK<sup>+</sup>). We observed severe morphological changes of the cortical actin cytoskeleton accompanied by impairments in the rate of phagocytosis and in chemotactic motility. In addition, we directly monitored the influence of MyoK expression on the maintenance of resting cortical tension. Altogether, the results underline a link between the potential molecular function of MyoK as actin-crosslinker and its distinctive involvement in cortical management.

## MATERIALS AND METHODS

### Cell culture

*Dictyostelium discoideum* AX2 cells were grown in HL5c nutrient medium (Sussman, 1987) supplemented with 100 i.u./ml Penicillin-Streptomycin (GibcoBRL), *myoK*<sup>-</sup> cells were maintained with 5 µg/ml Blasticidin S (Calbiochem) and the MyoK<sup>+</sup> cells with 5 µg/ml Geneticin (GibcoBRL).

### *Dictyostelium discoideum* transformation

Transformation was carried out according to Howard et al. (1988) and Kuspa and Loomis (1992) with slight modifications. After electroporation, selection was applied for 24 hours with Blasticidin S at 10 µg/ml or Geneticin at 10 µg/ml, and continued with 5 µg/ml. Colonies were picked with a pipet tip and cells cloned by limiting dilution on *Klebsiella* plates (Sussman, 1987).

### Preparation of genomic DNA and total RNA from *Dictyostelium discoideum*

Preparation of genomic DNA and total RNA was performed as described previously (Schwarz et al., 1999).

### Southern and northern blotting

Southern and northern blotting were performed as described by Sambrook et al. (1989). DNA was transferred to nylon membranes (Hybond-N+, Amersham). Probes were labelled non-radioactively with digoxigenin-11-dUTP (DIG). The hybridization procedure was carried out as described by Roche Molecular Biochemicals, using high-SDS buffer for prehybridization and hybridization at 42°C, and

CDP-*Star* as detection substrate. RNA gels were transferred to Biotodyne B membranes (PALL), and equal loading was checked by Methylene Blue staining. Probes were radioactively labelled with [ $\gamma$ -<sup>32</sup>P]dATP by using the Random Primed DNA Labeling Kit (Roche Molecular Biochemicals). Membranes were crosslinked by UV (UV crosslinker, Amersham Life Science). Signals were either detected by X-ray films and subsequently scanned with Color OneScanner (Macintosh) or recorded and quantified by a Luminescent Image Analyzer LAS-1000 (FujiFilm).

### Generation of *myoK*<sup>-</sup> cells

A *myoK* 5' genomic clone starts 1362 bp upstream of the AUG start codon and ends at a single *Clal* site (nt 1734 within the cDNA). A central 801 bp *EcoRI* fragment was replaced by a Blasticidin resistance (*bsr*) cassette that had been excised by *EcoRI* digestion from the vector PBsR 503 (Putz and Zeng, 1998). 20 µg of the construct (digested with *XbaI* and *Clal* to release the vector backbone and dephosphorylated) were used for transformation. Resulting Blasticidin-resistant clones were screened by PCR with the following primer pair combinations (schematic position indicated in Fig. 3A). Either the K57.forw (5' TGCTGGTAAAACAGTCTCTGC 3'; nt 434-454 in the genomic sequence) or the *blast* (5' GTAAGTCCTTGTGGTATGTGTAGG 3'; nt 653-676 in the *bsr* cassette) sense primers were used in combination with the primer MG5.rev (3' GATGGTGAAGTTCAAAGTT 5', nt 3009-2191, lying downstream from the construct used for transformation) in the antisense orientation. Genomic DNA from *myoK*<sup>-</sup> clones gave rise to products of 2377 bp (K57.forw/MG5.rev) and 1610 bp (*blast*/MG5.rev) and that of non-homologous transformants to a product of 1776 bp (K57.forw/MG5.rev) and no product (*blast*/MG5.rev), respectively. Genomic DNA for PCR was purified using DNAzol (Molecular Research Center). Positive candidates were confirmed by Southern and western blotting.

### Generation of MyoK<sup>+</sup> cells

A full-length *myoK* cDNA was assembled by restriction and ligation of overlapping fragments from three cDNA clones. The coding sequence was then amplified by PCR using *Pfu* polymerase, 5' TGAGGTACCTTTCGTTTATTTTCATCAGGTG 3' as forward primer (omitting the start methionine and introducing a *KpnI* site, underlined) and 3' GTTCCATTTGTGAGTACTTTGTTTTA-CAGAATAAGTTAGAGCTCTGA 5' as reverse primer (omitting the stop codon and introducing a *XhoI* site, underlined). The PCR product was purified, cloned into the pCR-Script vector (Stratagene) and checked by sequencing. After digestion with *KpnI* and *XhoI* the *myoK* coding sequence was subcloned into the *D. discoideum* expression vectors carrying an N-terminal heptaHis-tag, pDXA-HC (Manstein et al., 1995) and an additional C-terminal Ty1 tag (Bastin et al., 1996), pDXA-HVTS. Positive clones were identified, linearized with *PvuI*, dephosphorylated and electroporated in AX2 cells. Transformants were cloned on *Klebsiella* plates and tested for expression by western blotting.

### Construction of the glutathione-S-transferase (GST)-GPR-loop fusion protein

The domain corresponding to 'loop1' of MyoK, the so called GPR-loop, located within nt 340-816 of the cDNA (TTA... TTT), was amplified by PCR using *Pfu* and 5' TATCCCGGGGATCCTT-ACAATATGTTACATCAGTATCAC 3' as sense primer and 3' GTCAACTACAACCTTGTATAATTTATTGAGCTCGGGCCCTAT 5' as antisense primer. The 498 bp PCR product was digested with *XmaI*, ligated in the corresponding site of pGEX-3X (Pharmacia) and controlled for orientation and sequence correctness.

### Expression of the GST fusion protein in *E. coli* and purification

Expression of the 43 kD GST fusion protein in BL-21 (DE3)

(Luderer-Gmach et al., 1996) was carried out according to Ausubel et al. (1997) with the following modifications. An overnight culture was grown at 37°C with 1% glucose and used to inoculate the main culture (1:20), which was then grown at 30°C to an OD<sub>600</sub> of 0.7. Expression was induced with 0.5 mM IPTG for 3 hours. Purification was carried out on a Glutathione-Sepharose 4B (Pharmacia) column following the manufacturer's instructions. During all purification steps, the protease inhibitor cocktail Complete (EDTA-free) was used (Roche Molecular Biochemicals).

### Antibodies

For immunofluorescence (IF) and western blotting experiments, the following antibodies were used: (1) anti-*D. discoideum* coronin (mAb 176-306-3; gift from Dr G. Gerisch, MPI for Biochemistry, Martinsried); (2) anti-*D. discoideum* plasma membrane glycoprotein (mAb V4C4F3, unpublished; gift from Dr J. Garin, CEA Grenoble); (3) a monoclonal antibody to the Ty1 tag (Bastin et al., 1996); (4) a rabbit polyclonal anti-GST antibody (Sigma). F-actin was visualized using 2 U of Texas Red- or Oregon Green-conjugated phalloidin (Molecular Probes) per coverslip. The antibody against MyoK was raised against the head fragment (Schwarz et al., 1999) expressed in *E. coli*. For western blotting, the anti-MyoK serum, diluted 1:4000 in 3% non-fat dry milk in TBS (150 mM NaCl, 50 mM Tris/Cl, pH 7.4) was cross-adsorbed to 1.75 mg protein from *myoK*<sup>-</sup> cells on a blotting membrane. For IF, the anti-MyoK serum, diluted 1:500 in PBS/0.2% gelatine, was cross-adsorbed to three coverslips of fixed *myoK*<sup>-</sup> cells. The secondary antibodies were goat-anti-mouse or goat-anti-rabbit IgGs conjugated to Cyanine 3.29-OSu (Cy3, Rockland) or to Alexa 488 (Molecular Probes) used at 1:500, or goat-anti-rabbit IgGs conjugated to HRP (BioRad), used at 1:2000.

### Microscopy techniques

Immunofluorescence were performed as described (Neuhaus et al., 1998) using an ultracold methanol fixation/permeabilisation. Alternatively, in order to visualize F-actin with phalloidin, cells were fixed with picric acid/paraformaldehyde (Humbel and Biegelmann, 1992) without the ethanol post-fixation. The antibodies were diluted in PBS/0.2% gelatine. Mounted samples were analyzed with an Axiophot 2 microscope (Zeiss) or a Leica confocal microscope DM/IRB using a 63× Plan-Apo objective with NA 1.40. Confocal optical sections were recorded at 200 nm per vertical step and eight times averaging. Image reconstruction and processing were carried out using the Huygens/Selima/Imaris software package from Bitplane AG (Zurich, Switzerland). For transmission EM, cells on sapphire coverslips were plunged in an ethane slush at -170°C, freeze-substituted and embedded in either Lowicryl or Epon (Neuhaus et al., 1998). Sections were observed in a Philips 400 T TEM.

### Quantitative analysis of morphological phenotypes

The plasma membrane staining with the 4C4 antibody was best suited to count the proportion of cells exhibiting exaggerated lamellipodia, whereas staining for the actin-associated protein coronin was best suited to score cells harboring excessive crown-like projections. Because they are both mouse monoclonal antibodies, we had to perform the staining on separate slides. In each case, a total of about 250-360 cells from at least two independent experiments were counted by two observers and compiled as presented in Table 1. The scoring of cells with exaggerated lamellipodia having accumulation of actin pads close to their ventral face (visualized by Oregon Green-phalloidin staining) required confocal scanning microscopy.

### Protein extracts and western blotting

After centrifugation cells were immediately lysed in sample buffer. Protein content was determined according to Bradford (1976) (BioRad). For western blotting, gels were transferred to nitrocellulose membranes (Protran, Schleicher & Schuell) and equal loading checked by Ponceau S staining. Primary and HRP-conjugated

secondary antibodies were diluted in 3% non-fat dry milk/TBS and incubated at room temperature. Use of ECL-Plus (Amersham) substrate and direct recording and densitometry by the Luminescent Image Analyser LAS-1000 (FujiFilm) allowed for quantification of signal intensities within a broad linear range.

### Triton-insoluble 'rigor' cytoskeletons

Triton-insoluble cytoskeletons were obtained according to Manstein and Hunt (1995), with the following modifications. 2×10<sup>8</sup> AX2 or MyoK<sup>+</sup> cells were used for each reaction. Cells were washed in Soerensen buffer (14.7 mM KH<sub>2</sub>PO<sub>4</sub> and 2 mM Na<sub>2</sub>HPO<sub>4</sub>, pH 6.0) and centrifuged at 500 g for 10 minutes at 2°C. Pellets were washed in 4 ml buffer (50 mM Tris/Cl, pH 8.1, 2.5 mM EDTA, 1 mM DTT, 5 mM benzamidine and Complete protease inhibitor cocktail containing 0.04% NaN<sub>3</sub>, and recentrifuged. Cells were then resuspended in 1.5 ml of buffer containing 5 U alkaline phosphatase (Roche Molecular Biochemicals), lysed by adding the same volume of buffer containing 1% Triton X-100 and by incubating for 10 minutes at room temperature and 1 hour on ice. The lysate was centrifuged for 15 minutes at 280,000 g and the pellet washed in buffer without NaN<sub>3</sub>. As control for the ATP-dependence, the same procedure was carried out in absence of NaN<sub>3</sub> and alkaline phosphatase but in presence of 10 mM Mg-ATP, 25 U/ml creatine phosphokinase (Sigma) and 20 mM creatine phosphate. The ATP-release was performed on the Triton-insoluble rigor cytoskeleton by resuspending the pellets under different salt conditions, using 200 µl release buffer (same buffer as above without NaN<sub>3</sub>) including 10 mM ATP and either 0, 100, 250 or 500 mM NaCl. After 5 minutes of incubation, the suspensions were centrifuged at 435,000 g for 10 minutes at 2°C. The ATP-release was repeated and the resulting supernatants pooled for analysis by western blotting with anti-MyoK antibodies.

### F-actin cosedimentation assay of the GST-GPR-loop construct

F-actin from rabbit skeletal muscle was purified according to Pardee and Spudich (1982). The sedimentation assay was performed as described by Jung and Hammer (1994) with minor modifications. Various amounts of the purified GST fusion protein were cosedimented with 4 µM F-actin in the absence of ATP. For the determination of the salt-dependency, 2 µM of the GST fusion protein was used and the final concentration of KCl was varied from 10 to 140 mM. Pellets and supernatants were analyzed by western blotting using anti-GST antibody at 1:10,000 and quantified as described above.

### Motility assay

The velocity of AX2, *myoK*<sup>-</sup> and MyoK<sup>+</sup> cells during chemotaxis was determined according to a standard procedure (Browning et al., 1995). The cyclic AMP (cAMP) gradients are established by the cells and their secreted phosphodiesterase activity, from different starting concentrations of cAMP.

### Streaming and development

The streaming assay was carried out according to Peterson et al. (1995). 1.5×10<sup>7</sup> cells were plated on a 6 cm Petri dish. Monitoring and documentation was carried out with a Zeiss Axiophot 2 microscope with a 20× Achromat objective.

### Phagocytosis of fluorescent yeasts

The phagocytosis assay was performed as described by Maniak et al. (1995) except that cells were assayed on substratum. *D. discoideum* cells were allowed to settle on coverslips. The protein content of each cell type was assessed at the start of the experiment and was found not to vary by more than 10% (data not shown). The experiment was started by addition of 100 µl medium containing the labeled yeasts at a 10:1 excess over the cells. At different time points, the coverslips

were shortly washed in 1× Soerensen, fixed in picric acid and embedded in Mowiol. At least 200 cells were analyzed on each coverslip with a Zeiss Axiophot 2 microscope, and ingested yeasts counted. The tetramethylrhodamine B isothiocyanate (TRITC) labeled yeasts were kindly provided by Dr M. Maniak (Kassel University).

### Micropipet aspiration assay

The theory and experimental basis for the micropipet aspiration assay to measure resting cortical tension was described by Yeung and Evans (1989) and applied to *D. discoideum* by Dai et al. (1999). Micropipets (borosilicate glass capillaries, R-series, World Precision Instruments) were pulled with a pipet puller P-97 (Sutter instruments) to a diameter of  $2.6 \pm 0.1 \mu\text{m}$ . Experiments were performed on an inverted Nikon microscope with a 40× Achromate objective, recorded with a CCD camera (Sony) and followed on a Panasonic monitor. Pictures were digitalized by NIH Image 1.57. Measurements on about 40 cells each of wild type, *myoK*<sup>-</sup> and *MyoK*<sup>+</sup>, were carried out in HL5c medium under gentle stirring to prevent cells from settling. Fresh cells were pipetted in the chamber every 10 to 20 minutes. Cells were held by the pipet and their diameter measured on a scale placed directly on the monitor. Then an increasing negative pressure was applied at a rate of 1.8 mbar/second (Air-Regulator, Sigmam) until the cells started to build a hemispherical deformation, at which point the pressure was dropped and the procedure repeated. The critical pressure values were validated when they could be measured at least twice for the same cell. Signals were recorded by 'Capacitance Recorder' and analyzed by 'WinPCA' software (A. W. H., unpublished). The cortical tension  $T_c$  can be derived from the critical pressure  $\Delta P$  as follows:  $\Delta P = 2T_c(1/R_p - 1/R_c)$ , where  $R_p$  and  $R_c$  are the radii of the pipet opening and the cell, respectively.

## RESULTS

### Evidence for a second actin binding site in MyoK, a novel type of myosin I

*MyoK* was first identified by a PCR screening strategy (Schwarz et al., 1999) and subsequently full-length cDNAs were obtained (AF090534). This gene was recently independently cloned by Sutoh and collaborators (Yazu et al., 1999). In order both to verify the unique features of the predicted primary structure of *MyoK* and to obtain enough sequence for gene targeting, the whole locus was cloned directly from unamplified, size-selected genomic sublibraries. In addition, the rapidly advancing genome project (Loomis, 1998) has produced shotgun sequences covering most of the *myoK* locus, confirming our data. *MyoK* has 858 amino acids and a predicted size of 94 kDa, making it one of the smallest myosins identified so far, except for some class XIV myosins (Heintzelmann and Schwartzmann, 1997; C. Hettmann, A. Herm, A. Geiter, B. Frank, E. C. S., T. S. and D. Soldati, unpublished). It has only a very short neck region (Fig. 1A) without a classical IQ motif (IQxxxRGxxxR; Rhoads and Friedberg, 1997) and, strikingly, virtually lacks a tail domain. Instead, *MyoK* has a 146 aa long insertion (GPR) within the head domain. Nevertheless, *MyoK* shows high homology to other class I myosins and carries a potential phosphorylation site in its actin-binding surface (Fig. 1A) obeying the TEDS rule (Bement and Mooseker, 1995).

In order to assess whether the unique features of the *MyoK* head domain influence the characteristics of binding to filamentous actin, we first performed crude cosedimentation assays of *MyoK* (endogenous and overexpressed) with Triton-

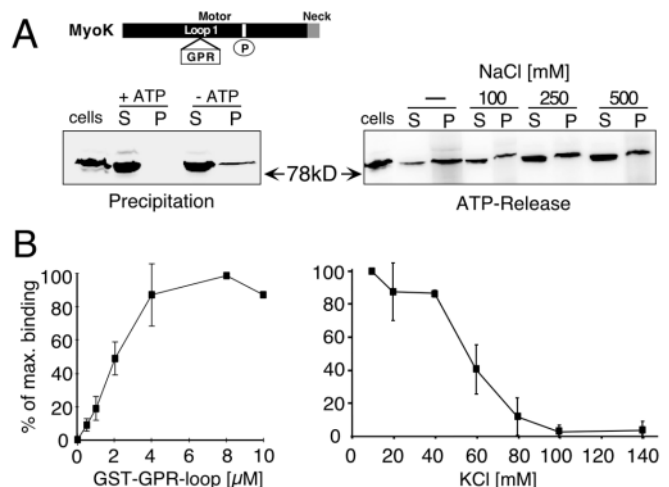
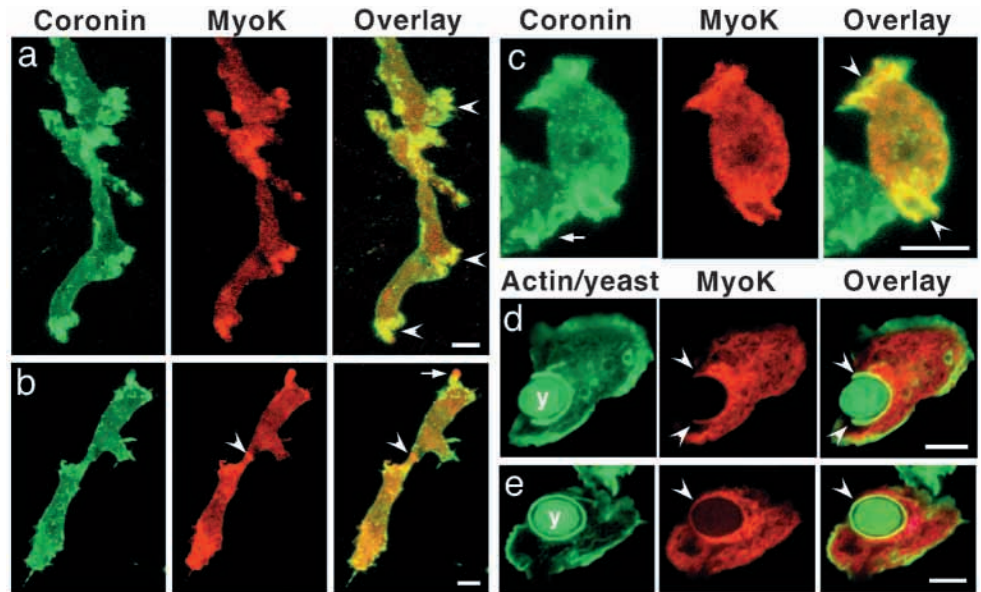


**Fig. 1.** Cosedimentation of *MyoK* and recombinant GST-GPR-loop with actin. (A) Model of *MyoK* protein highlighting the 146-amino-acid insertion (GPR-loop) and the TEDS phosphorylation site (P). Precipitation of *MyoK* with the Triton-insoluble cytoskeleton and ATP release. Cells were lysed in 0.5% Triton X-100 in the presence (+ATP) or in the absence (-ATP) of ATP and centrifuged. The pellet from the precipitation experiment (last lane, P in absence of ATP) was subsequently incubated in presence of 10 mM ATP to release myosins. The release was performed with ATP only (-) or with addition of ATP and increasing concentrations of salt (NaCl). Pellets (P) and supernatants (S) were analyzed by western blotting with the anti-*MyoK* antibody. The lane marked 'cells' is loaded with the same relative amount of lysate before centrifugation. (B) In vitro cosedimentation of the GST-GPR-loop with purified F-actin. (Left) A quantification of cosedimentation assays performed with different concentrations of GST-GPR-loop (0.5–10  $\mu\text{M}$ ) and 4  $\mu\text{M}$  F-actin at 10 mM KCl. After centrifugation, pellets and supernatants were analyzed by western blot. The percentage of maximal binding was plotted against the concentration of the GST-GPR-loop. 100% corresponds to approximately 2  $\mu\text{M}$  of bound GST chimera. (Right) A quantification of sedimentation assays carried out with 2  $\mu\text{M}$  of GST-GPR-loop and 4  $\mu\text{M}$  F-actin at different salt concentrations (10–140 mM KCl), quantified and plotted as in left panel.

insoluble cytoskeletons. Fig. 1A, left shows a representative result of such a sedimentation assay carried out in the presence and absence of ATP. More than 95% of the protein stayed in the supernatant when ATP was added. In absence of ATP, 30–40% of *MyoK* sedimented with the actin cytoskeleton. In order to ensure that the binding of *MyoK* to actin was reversible and correspondingly ATP-dependent, the rigor cytoskeleton was subsequently incubated in the presence of ATP and increasing salt concentrations up to 0.5 M (Fig. 1A, right). About 35% of *MyoK* was released from the pellet with ATP alone, and the amount was progressively increased up to 70% by the addition of salt. Detergents had no effect on the release efficiency (not shown). In contrast to myosin II, ATP alone does not release *MyoK* quantitatively from F-actin. An additional electrostatic interaction had to be disrupted by higher salt concentrations, which may reflect the presence of a second ATP-independent actin-binding site.

Sequence analysis also revealed that the *MyoK* loop1 (GPR-loop), rich in Gly (32%), Pro (21%) and Arg (10%), shows high similarity to the GPA and GPQ tail domains of other class I myosins, shown to bind actin in an ATP-independent manner.

**Fig. 2.** Intracellular localization of MyoK. MyoK was first visualized in wild-type developing cells (a). A similar distribution was also found in developing (b) and vegetative cells (c-e) of a line expressing low levels of a tagged-MyoK. MyoK was visualized either by anti-MyoK (a-c) or anti-Ty1-tag (d,e) antibodies. The localization of endogenous and tagged-MyoK is indistinguishable (compare a,b). In cells at the streaming stage of development (around 9 hours), MyoK and coronin, an actin-associated protein, were enriched with actin-rich protrusions (a, arrowheads) as well as at the leading edge (b, arrows). In addition, MyoK was found at cell-cell contacts (b, arrowhead). As already shown for other proteins expressed under the actin 15 promoter, a significant heterogeneity in the expression level is observed even in a clonal population of MyoK<sup>+</sup> cells (see the cell indicated by an arrow in c). In vegetative cells, coronin and MyoK localized to ruffles building macropinocytic cups (c, arrowheads). In cells fed with labeled yeast particles (y, in d,e), MyoK was enriched in phagocytic cups and partially colocalized with actin, as visualized by phalloidin staining (d,e, arrowheads). Bars, 5  $\mu$ m.



Therefore, we tested whether this loop also contains an actin-binding site. The GPR-loop was expressed in *E. coli* as a GST fusion protein and purified to homogeneity. Fig. 1B, left, presents the results of sedimentation assays with the GST-GPR-loop carried out in the presence of 4  $\mu$ M purified rabbit skeletal F-actin. The GPR-loop construct was found almost entirely in the pellet when used at low concentration. Binding was saturable and roughly corresponded to a 1:2 stoichiometry of GST-GPR-loop to actin, as at 4  $\mu$ M about half of the GPR-loop was found in the pellet. In addition, binding of the GPR-loop was salt-dependent (Fig. 1B, right). It decreased steadily from 40 mM to 80 mM KCl, and was completely abolished at higher salt concentrations. Negligible amounts of GPR-loop sedimented in absence of F-actin (not shown). Together, these results suggest that the head domain of MyoK possesses two actin-binding sites, a classical ATP-dependent one (Fig. 1A) and a secondary salt-dependent one (Fig. 1B).

### Subcellular localization of MyoK

Immunofluorescence analysis indicated that MyoK was distributed throughout the cytoplasm, with significant enrichment in dynamic regions of the actin cortex (Fig. 2). Due to the low expression level of endogenous MyoK in vegetative cells, cells expressing a tagged recombinant construct had to be used for unequivocal localization (Fig. 2b-e). However, the slightly higher expression level found naturally in developing cells (see also Fig. 6 and accompanying text) allowed detection of endogenous MyoK (Fig. 2a), and revealed that the localization of the overexpressed protein was indistinguishable from the endogenous one (compare Fig. 2a,b). MyoK colocalized with coronin, an actin-associated protein (de Hostos et al., 1991) at the periphery of both vegetative cells (Fig. 2c), as well as cells undergoing chemotactic streaming (Fig. 2a, arrowheads). In addition, in these developing cells MyoK was enriched at cell-cell contacts (Fig. 2b, arrowhead) or in rare peripheral regions devoid of coronin (Fig. 2b, arrow).

MyoK localized mostly to ruffles extending either to build macropinocytic cups called crowns (Fig. 2c, arrowheads) or to generate phagosomes during ingestion of yeast particles (Fig. 2d,e, arrowheads). Note that the colocalization with actin in these regions was manifest but not complete (Fig. 2d,e). Localization of MyoK at the actin cortex corroborates its potential actin-crosslinking function, but the significant cytosolic pool suggests that the localization (and activity) is probably strictly regulated.

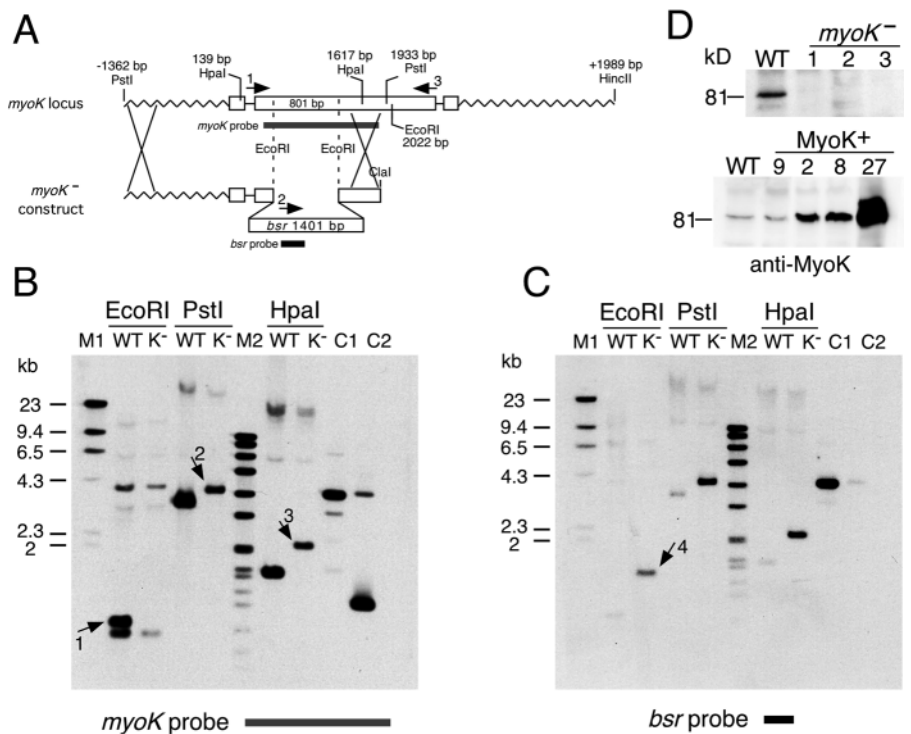
### Construction of MyoK mutant strains

In order to investigate the impact of different MyoK expression levels, we generated *myoK*<sup>-</sup> and MyoK<sup>+</sup> strains (Fig. 3). Three independent *myoK*<sup>-</sup> clones were subsequently confirmed by Southern blotting to have resulted from single homologous recombination events (Fig. 3B,C shows the analysis for one clone). Finally, absence of MyoK expression was confirmed by immunoblotting (Fig. 3D, upper panel). MyoK<sup>+</sup> strains were generated by stable integration of an expression vector with the entire MyoK cDNA under the control of a constitutive actin 15 promoter. Expression of MyoK in overexpressing strains was variable, reaching up to about 15 times the wild-type level (Fig. 3D, lower panel). The phenotypic analyses were initially performed on three independent *myoK*<sup>-</sup>, which behaved identically. The MyoK<sup>+</sup> clones showed more phenotypic heterogeneity, which seemed to correlate with the degree of MyoK expression. Subsequent analysis concentrated on high expressers. Note that individual MyoK<sup>+</sup> cells were heterogeneous even when derived from a single clone. The data presented here come from one representative clone of each: the *myoK*<sup>-</sup> clone 1 and MyoK<sup>+</sup> clone 27. The parent AX2 wild-type strain served as control.

### The morphology of the cortex is profoundly altered in MyoK mutant strains

Overall cell morphology was visualized by

**Fig. 3.** Generation and analysis of *myoK* mutant strains. (A) The genomic *myoK* locus is presented to scale. Restriction sites necessary for the interpretation of (B) and (C) are indicated. The construct for targeted disruption of the *myoK* gene is drawn below the locus (*myoK*<sup>-</sup> construct; *bsr*, blasticidin S resistance cassette). The positions of the *myoK* and the *bsr* DIG-labeled probe are indicated, as is the position of primers 1 (K57.forw), 2 (*blast*) and 3 (MG5.rev) used for a PCR diagnostic of gene disruption. The identity of the *myoK*<sup>-</sup> cells was confirmed by genomic Southern blotting. The blot was first hybridized with the *myoK* probe (B), and then with the *bsr* probe (C). When double crossover has occurred, the wild-type *EcoRI* fragment (801 bp, arrow 1) is replaced by the *bsr* resistance cassette and thus is missing in the *myoK*<sup>-</sup> cells. The *myoK* locus including the *bsr* cassette was 600 bp longer than in wild-type cells, resulting in longer *PstI* and *HpaI* fragments (B, arrows 2 and 3). The *bsr* probe hybridized only with DNA from *myoK*<sup>-</sup> cells, as for example after restriction with *EcoRI* (arrow 4). The very weak signal in the wild-type lane of the *PstI* restriction is due to incomplete stripping of the blot (compare the very strong signal when hybridized with the *myoK* probe in B). C1 and C2: 1 ng each of *myoK*<sup>-</sup> construct and *myoK* cDNA clone, respectively. Absence of expression of MyoK in *myoK*<sup>-</sup> cells was finally assessed by western blotting with anti-MyoK antibodies (D). The MyoK band present in wild-type cells (WT) is absent from the three independent *myoK*<sup>-</sup> clones (*myoK*<sup>-</sup> 1, 2 and 3, upper panel), and is increased from about 3- to 15-fold in different MyoK<sup>+</sup> clones (MyoK<sup>+</sup> 9, 2, 8 and 27, lower panel). Marker M2 in B and C has bands of the following sizes in kb: 8.0, 7.1, 6.0, 4.8, 3.5, 2.7, 1.9, 1.5, 1.4, 1.15, 1.0, 0.68, 0.49 from top to bottom.

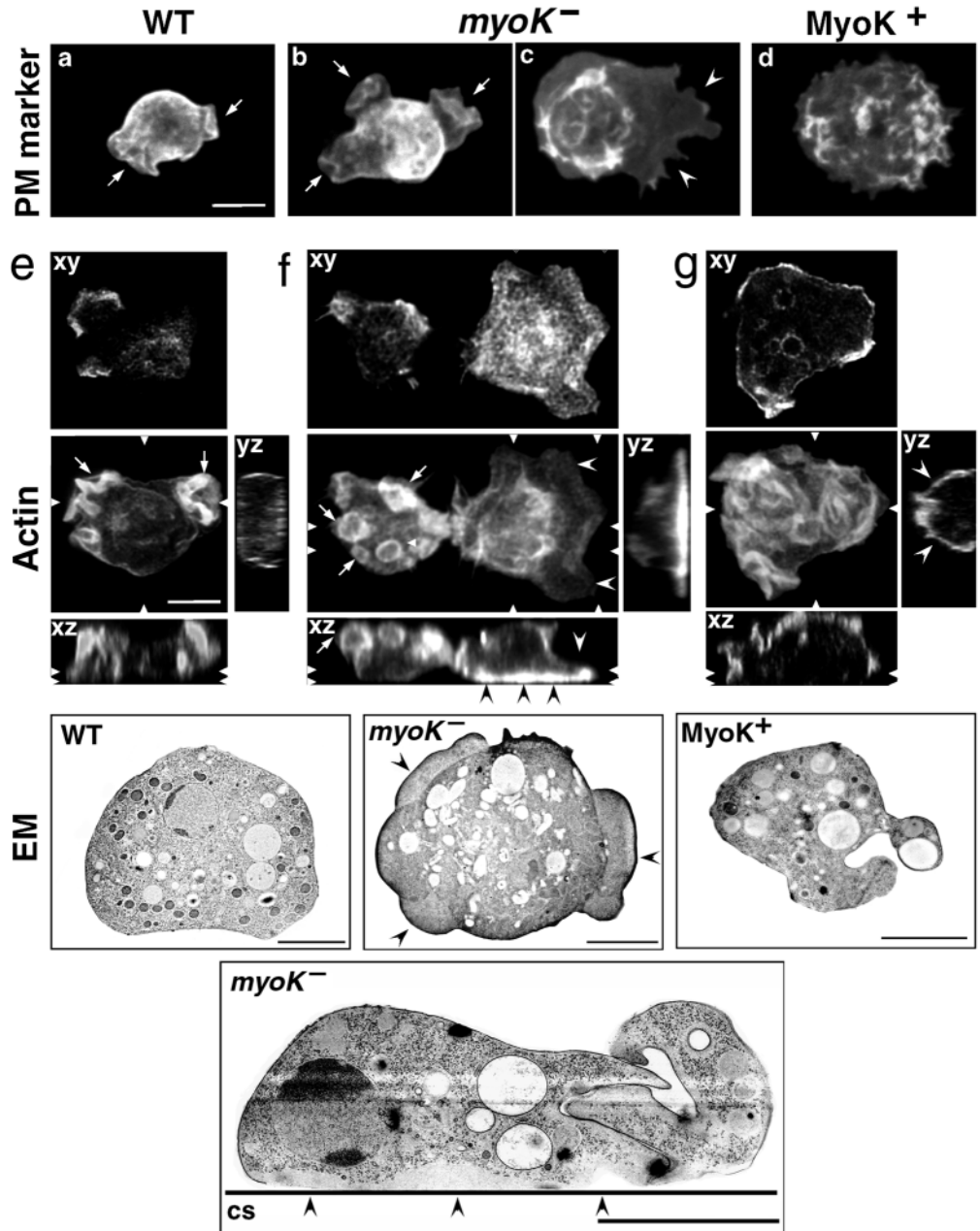


immunofluorescence staining against a plasma membrane glycoprotein, and representative examples of cells from each strain are shown in Fig. 4a-g. Extended focus projections of confocal stacks illustrated that wild-type cells were relatively smooth (Fig. 4a), except for the presence of few bowl-shaped structures called crowns (arrows) and the polarized extension of pseudopods. In sharp contrast, most *myoK*<sup>-</sup> cells displayed excessive ruffling, sometime in the form of crowns (Fig. 4b, arrows) or more characteristically as large, thin lamellipodia in their foot region (Fig. 4c, arrowheads). Many MyoK<sup>+</sup> cells displayed irregular shapes and a 'rougher' surface appearance (Fig. 4d). The extent of the disorders can be better appreciated after quantitative analysis of two morphological parameters, the number of crowns and the presence of lamellipodia (Table 1). Over 80% of wild-type cells exhibited between none and two crowns, whereas only 4.4% had more than 3. The *myoK*<sup>-</sup> cells showed over a fivefold increase in cells with more than three crowns, whereas MyoK<sup>+</sup> cells had a high proportion (12.3%) of cells with coronin-filled surface structures that were not classifiable as circular crowns. Concerning the appearance of lamellipodia, about two thirds of wild-type cells showed no such structure, and only 6.1% had prominent lamellipodia. Compared to this, *myoK*<sup>-</sup> cells showed a high, almost fivefold, increase in the proportion of cells exhibiting exaggerated flat ruffles. It is crucial to realize that the 58.3% of *myoK*<sup>-</sup> cells with the lowest number of crowns include the 27.3% of cells with excessive lamellipodia. The proportions of MyoK<sup>+</sup> cells with different degrees of lamellipodia were not distinguishable

from wild type. Therefore, over half of the *myoK*<sup>-</sup> cells exhibit a dramatic phenotype, whereas the morphological disturbances of MyoK<sup>+</sup> cells were evident but more difficult to capture in these numbers.

In order to assess whether the cortical cytoskeleton is correspondingly disturbed, we stained actin filaments with phalloidin. Fig. 4e-g shows a combination of projections and sections, parallel to the coverslip at the foot of the cell (Fig. 4xy) or perpendicular to the coverslip (Fig. 4yz and xz). In wild-type cells, most of the staining was concentrated in crowns and pseudopod extensions (Fig. 4e, arrows) and the ventral part of the cell was relatively depleted of F-actin (Fig. 4e, xy). Phalloidin staining of *myoK*<sup>-</sup> cells emphasized the exaggerated surface structures (Fig. 4f, crowns, arrows; lamellipodia, arrowheads) observed with plasma membrane staining. After deconvolution of confocal stacks and observation of perpendicular sections, it also became evident that most if not all cells with a flattened foot additionally exhibited F-actin 'pads' on their ventral surface (Fig. 4f, intense speckled staining in xy and black arrowheads in xz). In comparison, staining of MyoK<sup>+</sup> cells (Fig. 4g) showed a more rounded, contracted overall morphology with an almost continuous cortical F-actin shell (Fig. 4g). The surface of most MyoK<sup>+</sup> cells appeared very irregular with actin-driven short projections extending in all directions. As often observed in *D. discoideum* for protein expression driven by the actin 15 promoter, MyoK showed significant cell-to-cell variation, likely to be responsible for a phenotypic

**Fig. 4.** Morphology of MyoK mutant cells. (a-g) Confocal microscopy after fluorescence labelling of wild-type (WT, left), and MyoK mutant cells (*myoK*<sup>-</sup>, centre and MyoK<sup>+</sup>, right) against a plasma membrane marker (mAb 4C4, PM marker, a-d) and with Oregon Green phalloidin (Actin, e-g). (a-d) and the central panels in (e-g) present extended focus projections of the whole cell. The panels denoted xy, yz and xz show either single sections or projections of a few sections cut at the places marked by small white arrowheads on the left and right of the central projections (e-g). xy sections are taken at the foot of the cells. Sections yz and xz are taken perpendicularly to the coverslip. White arrows indicate some characteristic crown projections (a,b,e,f), whereas white arrowheads indicate thin, enlarged lamellipodia in *myoK*<sup>-</sup> cells (c,f) and continuous cortical staining in MyoK<sup>+</sup> cells (g). (EM) Electron micrographs of thin sections taken parallel to the coverslip (cs) at the foot of the cells (WT and *myoK*<sup>-</sup>) or in the middle of the cell height (MyoK<sup>+</sup>) or alternatively perpendicularly to substratum (*myoK*<sup>-</sup>, bottom). Black arrowheads indicate exaggerated lamellipodia and the presence of actin pads at the foot of the cell (*myoK*<sup>-</sup>). Both correspond to similar structures seen by confocal microscopy in c and f. Bars, 5  $\mu$ m.



heterogeneity (see Fig. 9 and accompanying text).

Finally, electron microscopy confirmed these morphological aberrations. In most wild-type cells, sections taken close to the cell foot revealed a relatively round circumference (Fig. 4, WT) with occasional lamellipodia. The enlarged lamellipodial structures of *myoK*<sup>-</sup> cells were clearly visible, contained no organelles and were apparently filled with F-actin (Fig. 4, *myoK*<sup>-</sup>). In addition, as already revealed by phalloidin staining, *myoK*<sup>-</sup> cells often exhibited thick actin pads close to the substratum (Fig. 4 bottom, *myoK*<sup>-</sup>, black arrowheads). The type of protrusion found in MyoK<sup>+</sup> cells totally differed from the enlarged lamellipodia of the knock-out cells because, as revealed by EM, they were filled with organelles (Fig. 4, MyoK<sup>+</sup>).

We conclude from these data that both the absence and superabundance of MyoK is detrimental to the integrity of the actin cortex. We then tested whether these alterations have consequences on cellular processes requiring dynamic remodeling of the cell periphery.

### Phagocytosis is reduced in MyoK mutant strains

We investigated the time-dependent uptake of TRITC-labelled yeasts. Such assays are usually performed on cells in suspension, but to maintain consistency with the morphological study, we examined adherent cells. On average, at early points, *myoK*<sup>-</sup> cells as well as MyoK<sup>+</sup> cells phagocytosed about 30% less yeast cells than the wild-type (Fig. 5). After 30 minutes, all three cell types reached a similar steady-state level of ingested yeasts, indicating that the defect resided mainly in initial uptake rates and not in the downstream processing of the phagosomes.

### MyoK expression is modulated during the developmental cycle

*D. discoideum* cells reach highest motility in early stages of starvation-induced aggregation, then form a multicellular

**Table 1. Quantitative analysis of morphological phenotypes**

Surface structure	Number	WT	<i>myoK</i> <sup>-</sup>	MyoK <sup>+</sup>
Crowns	0-2	80.9%*	58.3%§	75.5%
	3	14.7%	18.3%	11.1%
	≥4	4.4%	23.4%*	1.1%
	Disordered	NA	NA	12.3%*
Lamellipodia	-	63.2%*	33.4%	59.9%
	+	30.6%	39.3%	33.5%
	+++	6.1%	27.3%*	6.6%

Two morphological parameters were examined, the number of crowns and the presence of lamellipodia. Staining for the actin-associated protein coronin allowed rapid visual scoring of the number of circular crown projections. A number of MyoK<sup>+</sup> cells exhibited disordered surface projections clearly distinct from crowns. Plasma membrane staining with the 4C4 antibody best visualized the lamellipodia, which were classified as (-) non-existent, (+) small, or (+++) extensive. Because both antibodies are mouse monoclonal, the two structures were scored independently. In each case, 250-360 cells were counted and compiled as presented. Due to the separate way of scoring, the 58.3% of *myoK*<sup>-</sup> cells with lowest number of crowns (§) include the 27.3% of cells with excessive lamellipodia. Representative cells from the categories indicated by \* are shown in Fig. 4. NA, not applicable.

organism with coordinated motility, and finally differentiate into stalk and spore cells. As MyoK appears to maintain a close relationship with dynamic regions of the cell cortex, we investigated the expression of MyoK during the developmental cycle. Accumulation of *myoK* mRNA was highest after about 2 hours of starvation, and decreased almost linearly until 14-16 hours. Only very little transcript was detected in the latest stages, from 18 to 24 hours (Fig. 6A). It has been reported that cells growing in axenic cultures correspond to a developmental stage from about 2 to 4 hours, probably explaining the slight discrepancy between the lane loaded with RNAs extracted from axenically growing cells and the one loaded with truly vegetative cells grown on a bacterial lawn (Fig. 6A, compare lane axenic with 0 hours). Protein expression showed a corresponding dependence on the developmental stage. MyoK expression peaked between 6 and 10 hours, when cells reached their highest motility. Then, the steady state level of MyoK did not decrease linearly, but instead fell abruptly from 100% to 13% at 12 hours, the final step of aggregation (Fig. 6B). In parallel with the mRNA level, very little protein is detectable at later stages.

### MyoK<sup>-</sup> cells show a delay in aggregation

The doubling times of different *myoK*<sup>-</sup> strains grown in suspension and on plates were comparable to values obtained for wild-type cells. Also, *myoK*<sup>-</sup> cells completed their developmental cycle in about 24-26 hours, and the final basal disk, stalk and fruiting body were morphologically indistinguishable from wild type (Fig. 7). These results are in agreement with the findings of Yazu and coworkers (1999). Nevertheless, closer examination of the early stages of development corresponding to the chemotactic aggregation phase revealed a significant difference. On a confluent Petri dish wild-type cells normally start streaming after 7 hours in starvation buffer. Interestingly, wild-type and *myoK*<sup>-</sup> strains plated under the same conditions showed no significant difference during the first hours. But after 10 hours, the wild-type strain had built long chains of cells, while the null cells

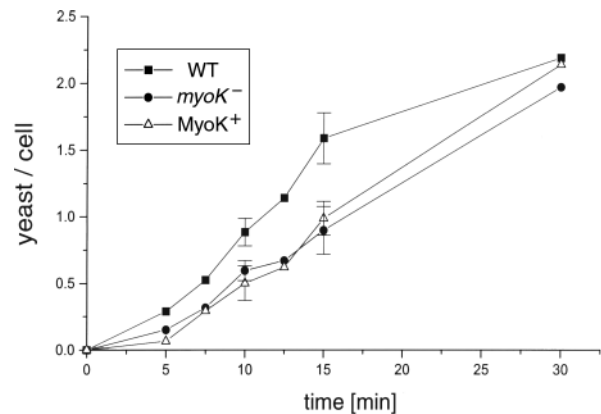


**Fig. 5.** Phagocytosis of TRITC-labeled yeast by adherent *D. discoideum* cells. Cells were plated on coverslips, fed with yeasts and fixed. The average number of yeasts ingested per wild-type (WT), *myoK*<sup>-</sup> and MyoK<sup>+</sup> cell is plotted against time. At least 200 *D. discoideum* cells were analyzed for each time point.

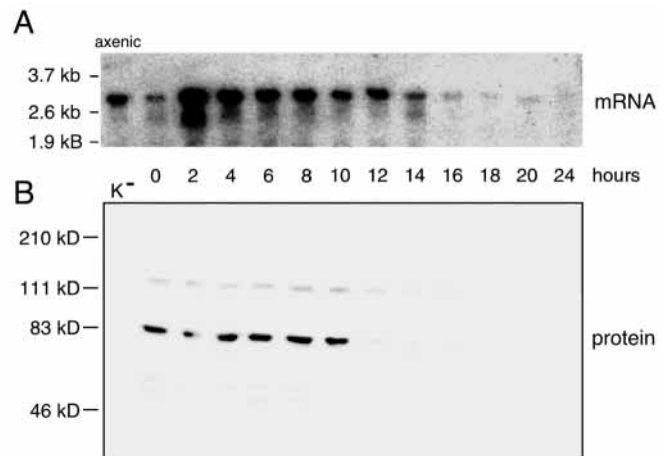


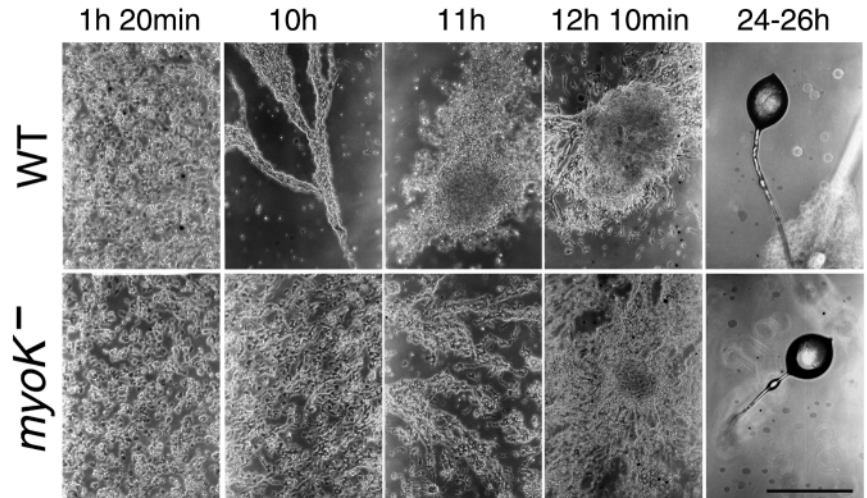
**Fig. 6.** Expression of MyoK is developmentally regulated. The developmental cycle of *D. discoideum* is completed in 24 hours. (A) A representative result of a northern blot hybridized with the *myoK* probe (see Fig. 3A). (B) Expression of MyoK protein at corresponding time points was analyzed by western blotting with the anti-MyoK antibody. In addition to the strong MyoK signal, a single faint cross-reacting band was visible around 120 kDa. Axenic cells were grown in liquid culture. K<sup>-</sup>, *myoK*<sup>-</sup> cells.

had only elongated and barely started streaming. After about 11 hours, wild-type cells had formed aggregates. In contrast, the null strain was starting to stream in long chains of cells, roughly similar to the 9-10 hour stage of the wild-type cells. Wild-type aggregates reached a compact stage after about 12 hours, while at the same time *myoK*<sup>-</sup> cells reached the early aggregate stage. Taken together, these and similar observations indicated that cells unable to express MyoK suffered a delay of 2-3 hours in early development. No developmental defect was apparent in MyoK<sup>+</sup> cells (not shown).

### MyoK<sup>-</sup> cells are reduced in motility

In order to investigate whether the delay in early development is related to a reduced velocity or to an impairment in signal

**Fig. 7.** The *myoK*<sup>-</sup> cells are delayed about 2 hours in early development. The streaming assay was performed in parallel with wild-type (WT) and *myoK*<sup>-</sup> cells. Identical numbers of cells were plated in starvation buffer and monitored by light microscopy. Phase-contrast pictures of the developmental stages were taken at the indicated time points. Bar, 250  $\mu\text{m}$ .



transduction, we monitored the influence of artificial alterations of MyoK levels on chemotactic motility. Using a standard chemotaxis motility assay, we analyzed the velocity of *myoK*<sup>-</sup> and MyoK<sup>+</sup> cells in cAMP gradients established by the cells themselves through secretion of phosphodiesterase. First, the fact that the motility of all three cell lines peaked at the same cAMP concentration was strong evidence that signal transduction was not impaired in MyoK mutant strains (Fig. 8). Reduced phosphodiesterase activity or lower sensitivity to cAMP would result in the shift of the curve maximum to higher concentrations, but cells would finally reach maximal velocity. In sharp contrast, *myoK*<sup>-</sup> cells exhibited only half the velocity (6  $\mu\text{m}/\text{minute}$ ) of wild-type cells (13  $\mu\text{m}/\text{minute}$ ), while the motility of the MyoK<sup>+</sup> cells remained unchanged (Fig. 8), indicating that reducing the concentration of MyoK induced a significant motility defect.

### The resting cortical tension directly correlates with the expression of MyoK

The close apposition and linkage of the cortical actin cytoskeleton to the plasma membrane is thought to be primarily responsible for the maintenance and regulation of resting cortical tension. Different setups have been used to measure the membrane tension, including the micropipet aspiration technique. The method is based on the mathematical modeling of cells in suspension as a reversibly deformable liquid core encapsulated by a cortical shell (Yeung and Evans, 1989), which was recently shown to be applicable to the study of neutrophils (Zhelev et al., 1994) and *D. discoideum* (Dai et al., 1999). We adapted a setup to allow for the measurement of the minimal critical pressure necessary to induce a hemispherical deformation of the cell surface (Fig. 9A). The values obtained for each strain were plotted as histograms and fitted to Gaussian curves. Whereas the response of wild-type and *myoK*<sup>-</sup> cells was homogeneous and corresponded to mean critical pressures of  $52.54 \pm 1.67$  mbar and  $40.64 \pm 1.62$  mbar, respectively (mean  $\pm$  s.e.m.), MyoK<sup>+</sup> cells were heterogeneous, as visualized by the presence of two maxima. Therefore, the MyoK<sup>+</sup> cells were subdivided into two populations with a mean critical pressure of  $55.46 \pm 1.51$  mbar and of  $88.26 \pm 7.57$  mbar, respectively. The first group is not statistically different from wild-type cells, but the second reached a value 70% higher than wild type, the opposite of the 24% lower pressure found for *myoK*<sup>-</sup> cells. An unpaired *t*-test indicated that the differences between these three cell lines are highly significant at the level of 0.1%. Knowledge of the radii of the cells and of the micropipet opening ( $2.6 \pm 0.1$   $\mu\text{m}$ ) allowed us to calculate values for the cortical tension itself, according to the liquid-drop model. Wild-type, *myoK*<sup>-</sup> and

MyoK<sup>+</sup> cells have a mean cortical tension of 4.33, 3.31 and 7.34 dyn/cm, for diameters of  $11.5 \pm 1.37$ ,  $11.9 \pm 1.44$  and  $11.1 \pm 1.51$   $\mu\text{m}$ , respectively. These values are about 100-fold higher than those found for neutrophils and other granulocytes (Evans and Yeung, 1989; Zhelev and Hochmuth, 1995) but in good agreement with those already reported for a few *D. discoideum* strains (Pasternak et al., 1989; Egelhoff et al., 1996; Dai et al., 1999).

### DISCUSSION

Class I myosins play essential roles in motile cells as ‘caretakers’ or managers of the cortex. Among the seven class I myosins expressed in *D. discoideum*, the novel myosin IK is distinguished by its unusual structure. Motor domains are

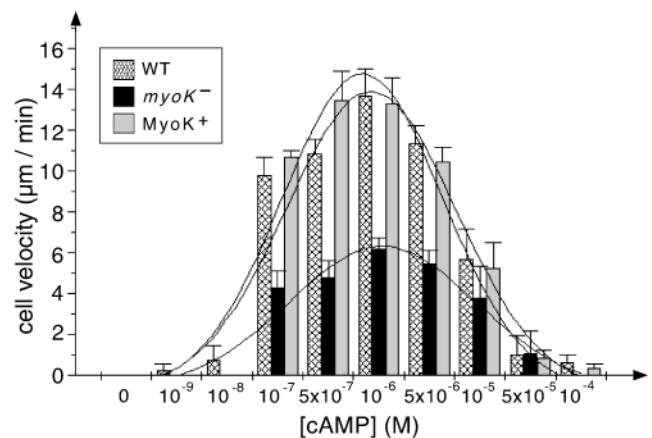
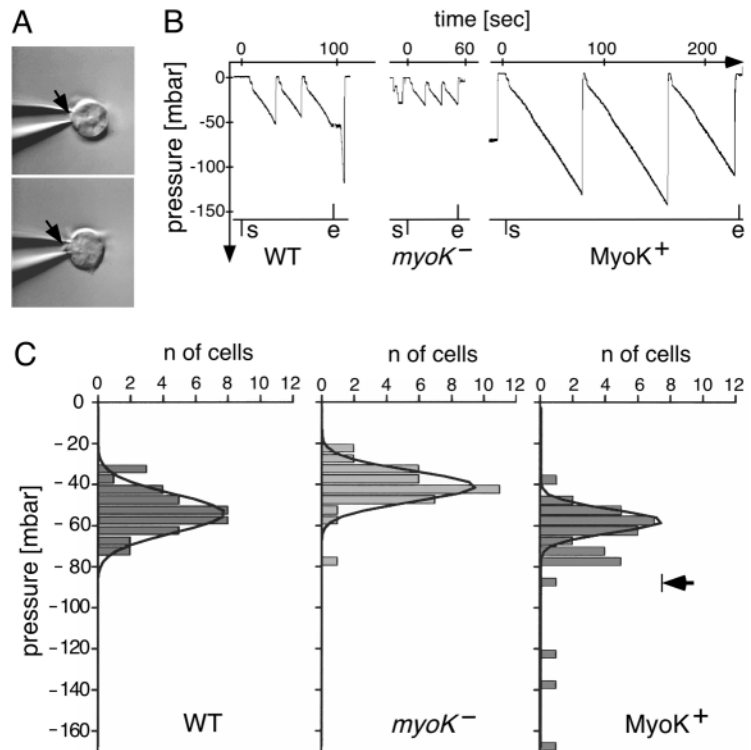


**Fig. 8.** Chemotactic motility of wild-type, *myoK*<sup>-</sup> and MyoK<sup>+</sup> cells. Aggregation competent cells from each type were deposited in a drop on agar plates containing different concentrations of cAMP. As a result of their secreted cyclic AMP-phosphodiesterase activity, *D. discoideum* cells hydrolyzed cAMP and thereby generated a gradient whose steepness depends on the concentration of cAMP in the surrounding agar. Cells thus spread radially from the original drop. The resulting average velocity of migration was plotted as a function of the different starting cAMP concentrations.

**Fig. 9.** Measurement of resting cortical tension. The resting cortical tension was measured by the micropipet aspiration technique. (A) Cells from a suspension were held by a pipet and their diameter measured. Then an increasing negative pressure was applied until the cells started to build a hemispherical deformation (arrows). (B) Representative pressure traces recorded from wild-type (WT), *myoK*<sup>-</sup> and MyoK<sup>+</sup> cells as a function of time. Each measurement began (start: s) with a zero holding pressure, which was then increased at a rate of 1.8 mbar/second, until the cells were deformed as shown in A, at which point the pressure was dropped and the procedure repeated. The critical pressure values were validated when they could be measured at least twice for the same cell before the experiment ended (end: e). (C) Histograms of the number of cells exhibiting a given critical pressure (total number was 38, 37 and 36 cells, respectively). For wild-type and *myoK*<sup>-</sup> cells, the histograms were fitted to single Gaussian curves corresponding to mean critical pressure of  $52.54 \pm 1.67$  mbar and  $40.64 \pm 1.62$  mbar, respectively (mean  $\pm$  s.e.m.). The responses of MyoK<sup>+</sup> cells were heterogeneous, as visualized in the histogram by the presence of two maxima, and were therefore sorted into two groups. One group was fitted to a Gaussian curve centered on a mean critical pressure of  $55.46 \pm 1.51$  mbar. The critical pressures from the other group were scattered around an average of  $88.26 \pm 7.57$  mbar (arrow). With the exception of the population of MyoK<sup>+</sup> cells with almost wild-type mean critical pressure, an unpaired *t*-test indicated that the differences between these three cell lines were highly significant at the level of 0.1%.



highly conserved and differences in length and sequence are usually confined to a few loci including the surface loops. MyoK carries an exceptional insertion in the surface loop1, which has been shown to modulate nucleotide exchange, the rate-limiting step controlling myosin velocity. The profound alteration resulting from the insertion in loop1 does not impair one of the central properties expected from a myosin, its ATP-dependent actin binding. MyoK is among the shortest myosins known to date. Due to the virtual absence of a neck and/or tail domain MyoK bears superficial resemblance with myosins of the apicomplexan parasites *Toxoplasma gondii* and *Plasmodium falciparum* (Heintzelman and Schwartzman, 1998). These myosins also lack recognisable light chain binding sites (IQ motifs) but carry a true tail domain which, in the case of TgMyoA, carries a di-lysine motif responsible for plasma membrane association (C. Hettmann, A. Herm, A. Geiter, B. Frank, E. C. S., T. S. and D. Soldati, unpublished). Nevertheless, despite its peculiarities, MyoK is definitively a myosin I, whereas the coccidian myosins are more divergent and build the class XIV of unconventional myosins. MyoK may be considered as a natural mutant possessing the minimal set of domains required for myosin I function in vivo.

#### Evidence that MyoK may be a novel type of regulated actin crosslinker

Analysis of the MyoK sequence also indicated that the GPR-loop resembles actin-binding domains usually found in the tail of other class I myosins. This GPR-loop was indeed shown to bind actin in an ATP-independent manner. Binding was sensitive to salt concentrations which are physiologically relevant, as the ionic strength of *D. discoideum* cytosol has been estimated to range from 40 to 80 mM salt equivalents

(Marin and Rothman, 1980; Steck et al., 1997). In addition, it is reasonable to assume that the interaction could well be even stronger in the context and geometry of the MyoK head domain compared to a GST fusion. In that respect, the fact that ATP-induced release of MyoK binding to F-actin is only facilitated but not rendered quantitative by salt concentrations as high as 250–500 mM is an additional indication that the interaction is relevant at physiological ionic strength. MyoK thus may possess two actin-binding sites within its motor domain, both of which are potential sites of regulation. First, MyoK is likely to be phosphorylated at its TEDS-site Thr residue, generating a negative charge at a conserved position within the actin contact region. According to the TEDS-rule (Bement and Mooseker, 1995), this residue is either an Asp (D) or Glu (E) or, as in myosins of the class I and VI, a Ser (S) or Thr (T). In lower eukaryotes, phosphorylation of this residue regulates the actin-activated ATPase and is crucial for function (Wu et al., 1996). The modification is carried out by myosin I heavy chain kinases (MIHCK) of the PAK65/Ste20 family (Brzeska et al., 1996), regulated by the GTP-bound form of small GTPases of the Rho/Rac/Cdc42 family (Lee et al., 1996). This signalling cascade underscores a direct link between myosin of the class I and the remodeling of the cytoskeleton mediated by these GTPases (Ridley, 1996). Second, the GPR-loop contains poly-Pro motifs known to bind profilin and VASP-like proteins, as well as a classical binding motif for SH3-containing proteins. In *D. discoideum*, profilin I and profilin II seem to be the major G-actin sequestering proteins (Noegel and Luna, 1995). Expression of both isoforms is developmentally regulated and the expression pattern of profilin I perfectly corresponds to MyoK expression profile (Haugwitz et al., 1991). Indeed, we have preliminary evidence that profilin and/or the profilactin

complex bind tightly to the GST-GPR-loop. These additional functions of the GPR-loop do not exclude the proposed actin-binding activity, but add a layer of complexity and regulation, as well as a potential link to the control of actin dynamics.

Accumulating evidence suggests that various class I myosins may cross-link actin in different manners. *Acanthamoeba* myosin IA and IB were reported to cross-link actin (Fujisaki et al., 1985), possibly through a secondary actin-binding site contained in their GPA tail domain. More recently, the study of *myr3*, a mammalian amoeboid myosin lacking a GPA domain, revealed that it nevertheless was able to cross-link actin (Stöffler and Bähler, 1998). The domain responsible has not been defined yet. We speculate that the natural design of MyoK, lacking tail domains but with its 'transposed' GPR actin-binding domain, may reveal a novel mode and geometry of actin cross-linking. The interaction with F-actin is ATP-dependent, but is likely regulated by additional factors. On one hand, the formation of a rigor complex was not quantitative. On the other hand, addition of ATP alone to this complex released about one third of MyoK, whereas addition of high salt was necessary to release another third. The remainder of MyoK seemed 'locked' in its interaction with actin. This apparent heterogeneity might reflect the influence of regulation by TEDS-site phosphorylation and by GPR-loop binding partners.

### Function of MyoK as a cortical cytoskeleton manager

MyoK localizes to dynamic regions of the actin cortex. Similar distributions have been reported for other class I myosins in *D. discoideum*, including enrichment in pseudopodia, phagocytic cups and at the leading edge (Ostap and Pollard, 1996b). Homologues of the amoeboid class I myosins were identified in vertebrates (Edgar et al., 1996; Stöffler et al., 1995; Bement et al., 1994). In NRK cells, *myr3* was found concentrated in ConcanavalinA-inducible F-actin-rich structures at regions of cell-cell contact (Stöffler et al., 1995). So far, database searching failed to identify MyoK-related sequences, but affinity-purified anti-MyoK antibodies detected a protein of the expected size in extracts from mouse heart, hinting at the existence of a MyoK homologue in a higher organism (data not shown).

The manipulation of MyoK expression levels gave insights into its function. *MyoK*<sup>-</sup> cells have aberrant morphology, showing an excess of ruffles, either extending on the back of the cells in the form of crowns, or even more characteristically on the substrate as enlarged lamellipodia. This phenotype is more severe than was described for other cell lines lacking a single myosin I (Novak et al., 1995; Jung et al., 1996; reviewed in Ostap and Pollard, 1996b) and is reminiscent of cells devoid of coronin, an actin-associated protein (de Hostos et al., 1993) and also of wild-type cells treated with intermediate doses of Cytochalasin A (our unpublished observations). The thick actin pads are very variable, but are clearly visible in cells with exaggerated lamellipodia. *MyoK*<sup>+</sup> cells adopt a rounder, more contracted morphology and have a 'rougher' surface with organelle filled protrusions. No significant difference was observed between the cell lines in the G- to F-actin ratio measured both in suspension and on substrate (not shown). Without shifting the equilibrium between G- and F-actin, the manipulation of MyoK levels affects the organisation of the

cortical actin cytoskeleton. This is remarkable because MyoK is not an abundant protein. This speaks both against functional redundancy and in favour of a distinctive function in cortical management.

How is this cortical management exerted and what are the cellular functions most directly affected or regulated by MyoK? We measured the resting cortical tension and found a direct correlation with the presence and level of MyoK. We thus suggest a working model in which MyoK, acting as a specialized actin-crosslinker, is an important regulator of the morphology of the cortical cytoskeleton. Absence of MyoK results in a thinner or more dynamic actin cortex, leading to a drop in cortical tension, which allows cells to more freely extend ruffles. Superabundance of MyoK leads to a somewhat opposite phenotype. Perhaps due to a thicker or more continuous actin shell, cells have higher cortical tension, and a more contracted overall appearance. Moreover, the fact that MyoK is the potential target for multiple regulations would allow the fine tuning and adaptation of the cortex to its multiple tasks requiring strength and plasticity, such as occurs during phagocytosis and motility.

The actomyosin cytoskeleton plays a major role in the initial stages of phagocytosis. *D. discoideum* cells disrupted in a myosin VII gene exhibit significant and exclusive defects in phagocytosis (Titus, 1999). When phagocytosis is measured in suspension, *myoB*<sup>-</sup> and *myoC*<sup>-</sup> cells show slight impairments at early stages (Jung et al., 1996), but the steady state levels of ingested particles are normal in all myosin I single and multiple mutants (Novak et al., 1995). In contrast, when measured in adherent *myoA*<sup>-</sup>/*B*<sup>-</sup> cells, the uptake rates are slower and the steady state level lower compared to wild-type cells (data not shown). Both *myoK* mutant strains exhibit reduced initial rates of phagocytosis on substratum but reach steady state levels similar to wild-type cells, indicating that the downstream processing of the ingested particles proceeds normally. The slower uptake kinetics observed in *myoK* mutant strains might therefore reflect difficulties in establishing suitable contact with particles or defects in engulfment, resulting from a disorganized actin cortex.

The motility of *myoK*<sup>-</sup> cells was slowed, resulting in a delay of about 2 hours in chemotactic aggregation. Despite a higher cortical tension, *MyoK*<sup>+</sup> cells showed no obvious motility defect. Our results suggest that a certain threshold tension is important for motility but an increase over wild type is not detrimental. Interestingly, very recent data (Novak and Titus, 1997; Dai et al., 1999) suggest a parallel between overexpression of *D. discoideum* MyoB and MyoC, higher resting cortical tension, and motility defects. More work is clearly required to clarify this issue. The expression of MyoK is modulated in agreement with a functional linkage to motile behavior, as it peaks during the phase of highest motility and drops rapidly during the final aggregation stage. At the protein level, MyoB shows a similar expression profile during the developmental cycle, whereas MyoC and MyoD are constitutively expressed (Jung et al., 1996). In addition, except for this delay, *myoK*<sup>-</sup> cells have no apparent morphological defects at later stages, whereas *myoA*<sup>-</sup> and *myoB*<sup>-</sup> strains develop fewer and smaller fruiting bodies (Peterson et al., 1995).

In summary, the investigation of MyoK underscores interesting parallel and differences between the morphological

and functional analyses of other *D. discoideum* strains with disruptions of single and multiple class I myosins. On the one hand, there are important phenotypic similarities concerning the disturbed morphology of the actin cortex, the effects on resting cortical tension and the potentially resulting endocytosis and motility defects. On the other hand, we want to emphasize that the severity of the phenotypes is stronger in *myoK*<sup>-</sup> cells, as such defects were only observed in multiply disrupted strains. Moreover, there are specific differences as for example *myoK*<sup>-</sup> cells do not exhibit the pinocytosis defects seen in other mutants.

In the present study, we characterized a novel type of myosin, *D. discoideum* myosin IK, sharing structural features with class I myosins, but distinguished by an unusual architecture, which suggests that it might function as a novel class of regulated actin-crosslinker. Despite the presence of six other class I myosins in *D. discoideum*, both the absence and superabundance of MyoK resulted in severe defects of the actin cortex and affected cellular functions such as phagocytosis and motility. MyoK thus appears to have a distinctive role in cortical management.

Special thanks go to Dr M. Titus (University of Minnesota) for her assistance and guidance at many stages of the project, and also to Dr M. Knetsch for performing the chemotactic motility assay, for helpful comments and for careful reading of the manuscript. We also thank J. Bollmann for help with the imaging of aspirated cells, Dr D. Madden for careful reading of the manuscript, G. Helmig for preparing rabbit muscle acetone powder, and U. Buhre and J. Schleich for excellent technical assistance. Dr F. Puta (Charles University, Prag) generously provided vectors prior to publication. We thank Drs J. Garin (CEA Grenoble) and G. Gerisch (MPI for Biochemistry, Martinsried) for kindly providing antibodies. E.C.S. and the work presented here were supported by a grant from the DFG (SFB 352). E.M.N. and C.K. were recipients of doctoral fellowships from the Max-Planck-Gesellschaft.

## REFERENCES

- Adams, R. J. and Pollard, T. D. (1989). Binding of myosin I to membrane lipids. *Nature* **340**, 565-568.
- Ausubel, F. M., Brent, R., Kingston, R. E., Moore, D.D., Seidman, J. G., Smith, J. A. and Struhl, K. (1997). *Current Protocols in Protein Science*. In *Current Protocols in Molecular Biology*, Vol. 1. John Wiley and Sons, New York.
- Bastin, P., Bagherzadeh, A., Matthews, K. R. and Gull, K. (1996). A novel epitope tag system to study protein targeting and organelle biogenesis in *Trypanosoma brucei*. *Mol. Biochem. Parasitol.* **77**, 235-239.
- Bement, W. M. and Mooseker, M. S. (1995). TEDS rule: A molecular rationale for differential regulation of myosin by phosphorylation of the heavy chain head. *Cell Motil. Cytoskel.* **31**, 87-92.
- Bement, W. M., Wirth, J. A. and Mooseker, M. S. (1994). Cloning and mRNA expression of human unconventional myosin-1C. A homologue of amoeboid myosins-I with a single IQ motif and an SH3 domain. *J. Mol. Biol.* **243**, 356-363.
- Bradford, M. M. (1976). A rapid and sensitive method for the quantitation of microgram quantities of protein utilizing the principle of protein-dye binding. *Anal. Biochem.* **72**, 248-254.
- Browning, D. D., The, T. and O'Day, D. H. (1995). Comparative analysis of chemotaxis in *Dictyostelium* using a radial bioassay method: protein tyrosine kinase activity is required for chemotaxis to folate but not to cAMP. *Cell. Signal.* **7**, 481-489.
- Brzeska, H., Szczepanowska, J., Hoey, J. and Korn, E. D. (1996). The catalytic domain of *Acanthamoeba* myosin I heavy chain kinase. II. Expression of active catalytic domain and sequence homology to p21-activated kinase (PAK). *J. Biol. Chem.* **271**, 27056-27062.
- Dai, J., Ting-Beall, H. P., Hochmuth, R. M., Sheetz, M. P. and Titus, M. A. (1999). Myosin I contributes to the generation of resting cortical tension. *Biophys. J.* **77**, 1168-1176.
- de Hostos, E. L., Bradtke, B., Lottspeich, F., Guggenheim, R. and Gerisch, G. (1991). Coronin, an actin binding protein of *Dictyostelium discoideum* localized to cell surface projections, has sequence similarities to G protein beta subunits. *EMBO J.* **10**, 4097-4104.
- de Hostos, E. L., Rehfuess, C., Bradtke, B., Waddell, D. R., Albrecht, R., Murphy, J. and Gerisch, G. (1993). *Dictyostelium* mutants lacking the cytoskeletal protein coronin are defective in cytokinesis and cell motility. *J. Cell Biol.* **120**, 163-173.
- Edgar, A. J., Knight, A. E. and Bennett, J. P. (1996). Chicken myosin IB mRNA is highly expressed in lymphoid tissues. *J. Anat.* **189**, 451-456.
- Egelhoff, T. T., Naismith, T. V. and Brozovich, F. V. (1996). Myosin-based cortical tension in *Dictyostelium* resolved into heavy and light chain-regulated components. *J. Mus. Res. Cell Mot.* **17**, 269-274.
- Evans, E. and Yeung, A. (1989). Apparent viscosity and cortical tension of blood granulocytes determined by micropipet aspiration. *Biophys. J.* **56**, 151-160.
- Fujisaki, H., Albanesi, J. P. and Korn, E. D. (1985). Experimental evidence for the contractile activities of *Acanthamoeba* myosins IA and IB. *J. Biol. Chem.* **260**, 11183-11189.
- Furch, M., Geeves, M. A. and Manstein, D. J. (1998). Modulation of actin affinity and actomyosin adenosine triphosphatase by charge changes in the myosin motor domain. *Biochem.* **37**, 6317-6326.
- Hammer, J. A. III, Albanesi, J. P. and Korn, E. D. (1983). Purification and characterization of a myosin I heavy chain kinase from *Acanthamoeba castellanii*. *J. Biol. Chem.* **258**, 10168-10175.
- Hammer, J. A. III, Sellers, J. R. and Korn, E. D. (1984). Phosphorylation and activation of smooth muscle myosin by *Acanthamoeba* myosin I heavy chain kinase. *J. Biol. Chem.* **259**, 3224-3229.
- Haugwitz, M., Noegel, A. A., Rieger, D., Lottspeich, F. and Schleicher, M. (1991). *Dictyostelium discoideum* contains two profilin isoforms that differ in structure and function. *J. Cell Sci.* **100**, 481-489.
- Hayden, S. M., Wolenski, J. S. and Mooseker, M. S. (1990). Binding of brush border myosin I to phospholipid vesicles. *J. Cell Biol.* **111**, 443-451.
- Heintzelman, M. B. and Schwartzman, J. D. (1997). A novel class of unconventional myosins from *Toxoplasma gondii*. *J. Mol. Biol.* **271**, 139-146.
- Howard, P. K., Ahern K. G. and Firtel, R. A. (1988). Establishment of a transient expression system for *Dictyostelium discoideum*. *Nucl. Acids Res.* **16**, 2613-2623.
- Humbel, B. M. and Biegelmann, E. (1992). A preparation protocol for postembedding electron microscopy of *Dictyostelium discoideum* cells with monoclonal antibodies. *Scanning Microsc.* **6**, 817-825.
- Jung, G. and Hammer, J. A. III. (1990). Generation and characterization of *Dictyostelium* cells deficient in a myosin I heavy chain isoform. *J. Cell Biol.* **110**, 1955-1964.
- Jung, G. and Hammer, J. A. III. (1994). The actin binding site in the tail domain of *Dictyostelium* myosin IC (myoC) resides within the glycine- and proline-rich sequence (tail homology region 2). *FEBS Lett.* **342**, 197-202.
- Jung, G., Wu, X. F. and Hammer, J. A. III. (1996). *Dictyostelium* mutants lacking multiple classic myosin I isoforms reveal combinations of shared and distinct functions. *J. Cell Biol.* **133**, 305-323.
- Kuspa, A. and Loomis, W. F. (1992). Tagging developmental genes in *Dictyostelium* by restriction enzyme-mediated integration of plasmid DNA. *Proc. Natl. Acad. Sci. USA* **89**, 8803-8807.
- Lee, S. F., Egelhoff, T. T., Mahasneh, A. and Côté, G. P. (1996). Cloning and characterization of a *Dictyostelium* myosin I heavy chain kinase activated by Cdc42 and Rac. *J. Biol. Chem.* **271**, 27044-27048.
- Loomis, W. F. (1998). The *Dictyostelium* Genome Sequencing Project. *Protist* **149**, 209-212.
- Luderer-Gmach, M., Liebig, H. D., Sommergruber, W., Voss, T., Fessl, F., Skern, T. and Kuechler, E. (1996). Human rhinovirus 2A proteinase mutant and its second-site revertants. *Biochem. J.* **318**, 213-218.
- Maniak, M., Rauchenberger, R., Albrecht, R., Murphy, J. and Gerisch, G. (1995). Coronin involved in phagocytosis: Dynamics of particle-induced relocalization visualized by a green fluorescent protein tag. *Cell* **83**, 915-924.
- Manstein, D. J. and Hunt, D. M. (1995). Overexpression of myosin motor domains in *Dictyostelium*: screening of transformants and purification of the affinity tagged protein. *J. Muscle Res. Cell Motil.* **16**, 325-332.
- Manstein, D. J., Schuster, H. P., Morandini, P. and Hunt, D. M. (1995).

- Cloning vectors for the production of proteins in *Dictyostelium discoideum*. *Gene*. **162**, 129-134.
- Marin, F. T. and Rothman, F. G.** (1980). Regulation of development in *Dictyostelium discoideum*: IV. Effect of ions on the rate of differentiation and cellular response to cyclic AMP. *J. Cell Biol.* **87**, 823-827.
- Mayer, B. J.** (1997). Signal transduction: clamping down on Src activity. *Curr. Biol.* **7**, R295-298.
- Mermall, V., Post, P. L. and Mooseker, M. S.** (1998). Unconventional myosins in cell movement, membrane traffic, and signal transduction. *Science* **279**, 527-533.
- Miyata, H., Bowers, B. and Korn, E. D.** (1989). Plasma membrane association of *Acanthamoeba* myosin I. *J. Cell Biol.* **109**, 1519-1528.
- Murphy, C. T. and Spudich, J. A.** (1998). *Dictyostelium* myosin 25-50k loop substitutions specifically affect ADP release rates. *Biochem.* **37**, 6738-6744.
- Neuhaus, E., Horstmann, H., Almers, W., Maniak, M. and Soldati, T.** (1998). Ethane-freezing/methanol-fixation of cell monolayers. A procedure for improved preservation of structure and antigenicity for light and electron microscopies. *J. Struct. Biol.* **121**, 326-342.
- Noegel, A. A. and Luna, J. E.** (1995). The *Dictyostelium* cytoskeleton. *Experientia* **51**, 1135-1143.
- Novak, K. D., Peterson, M. D., Reedy, M. C. and Titus, M. A.** (1995). *Dictyostelium* myosin I double mutants exhibit conditional defects in pinocytosis. *J. Cell Biol.* **131**, 1205-1221.
- Novak, K. D. and Titus, M. A.** (1997). Myosin I overexpression impairs cell migration. *J. Cell Biol.* **136**, 633-647.
- Ostap, E. M. and Pollard, T. D.** (1996a). Biochemical kinetic characterization of the *Acanthamoeba* myosin-I ATPase. *J. Cell Biol.* **132**, 1053-1060.
- Ostap, E. M. and Pollard, T. D.** (1996b). Overlapping functions of myosin-I isoforms? *J. Cell Biol.* **133**, 221-224.
- Pardee, J. D. and Spudich, J. A.** (1982). Purification of muscle actin. *Methods Cell Biol.* **24**, 271-289.
- Pasternak, C., Spudich, J. A. and Elson, E. L.** (1989). Capping of surface receptors and concomitant cortical tension are generated by conventional myosin. *Nature* **341**, 549-551.
- Peterson, M. D., Novak, K. D., Reedy, M. C., Ruman, J. I. and Titus, M. A.** (1995). Molecular genetic analysis of myoC, a *Dictyostelium* myosin I. *J. Cell Sci.* **108**, 1093-1103.
- Pollard, T. D. and Korn, E. D.** (1973). *Acanthamoeba* myosin. I. Isolation from *Acanthamoeba castellanii* of an enzyme similar to muscle myosin. *J. Biol. Chem.* **248**, 4682-4690.
- Probst, F. J., Fridell, R. A., Raphael, Y., Saunders, T. L., Wang, A., Liang, Y., Morell, R. J., Touchman, J. W., Lyons, R. H., Noben-Trauth, K., Friedman, T. B. and Camper, S.** (1998). Correction of Deafness in *shaker-2* Mice by an Unconventional Myosin in BAC Transgene. *Science* **280**, 1444-1447.
- Puta, F. and Zeng, C.** (1998). Blastocidin resistance cassette in symmetrical polylinkers for insertional inactivation of genes in *Dictyostelium*. *Fol. Biol.* **44**, 185-188.
- Rayment, I., Rypniewski, W. R., Schmidt-Base, K., Smith, R., Tomchick, D. R., Benning, M. M., Winkelmann, D. A., Wesenberg, G. and Holden, H. M.** (1993). Three-dimensional structure of myosin subfragment-1: a molecular motor. *Science* **261**, 50-58.
- Rhoads, A. R. and Friedberg, F.** (1997). Sequence motifs for calmodulin recognition. *FASEB J.* **11**, 331-340.
- Ridley, A. J.** (1996). Rho: theme and variations. *Curr. Biol.* **6**, 1256-1264.
- Rosenfeld, S. S. and Rener, B.** (1994). The GPQ-rich segment of *Dictyostelium* myosin IB contains an actin binding site. *Biochem.* **33**, 2322-2328.
- Rosenfeld, S. S., Xing, J., Cheung, H. C., Brown, F., Kar, S. and Sweeney, H. L.** (1998). Structural and kinetic studies of phosphorylation-dependent regulation in smooth-muscle myosin. *J. Biol. Chem.* **273**, 28682-28690.
- Sambrook, J., Fritsch, E. F. and Maniatis, T.** (1989). *Molecular Cloning: A Laboratory Manual*. Cold Spring Harbor Laboratory Press, New York.
- Schwarz, E. C., Geissler, H. and Soldati, T.** (1999). A potentially exhaustive screening strategy reveals two novel divergent myosins in *Dictyostelium*. *Cell Biochem. Biophys.* **30**, 413-435.
- Sellers, J. R. and Goodson, H. V.** (1995). Motor proteins 2: myosin. *Prot. Profile.* **2**, 1323-1423.
- Spudich, J. A.** (1994). How molecular motors work. *Nature* **372**, 515-518.
- Steck, T. L., Chiaraviglio, L. and Meredith, S.** (1997). Osmotic homeostasis in *Dictyostelium discoideum*: Excretion of amino acids and ingested solutes. *J. Euk. Microbiol.* **44**, 503-510.
- Stöffler, H. E. and Bähler, M.** (1998). The ATPase activity of Myr3, a rat myosin I, is allosterically inhibited by its own tail domain and by Ca<sup>2+</sup>-binding to its light chain calmodulin. *J. Biol. Chem.* **273**, 14605-14611.
- Stöffler, H. E., Ruppert, C., Reinhard, J. and Bähler, M.** (1995). A novel mammalian myosin I from rat with an SH3 domain localizes to Con A-inducible, F-actin-rich structures at cell-cell contacts. *J. Cell Biol.* **129**, 819-830.
- Sussman, M.** (1987). Cultivation and synchronous morphogenesis of *Dictyostelium* under controlled experimental conditions. *Methods Cell Biol.* **28**, 9-29.
- Temesvari, L. A., Bush, J. M., Peterson, M. D., Novak, K. D., Titus, M. A. and Cardelli, J. A.** (1996). Examination of the endosomal and lysosomal pathways in *Dictyostelium discoideum* myosin I mutants. *J. Cell Sci.* **109**, 663-673.
- Titus, M. A.** (1999). A class VII unconventional myosin is required for phagocytosis. *Current Biol.* **9**, 1297-1303.
- Uyeda, T. Q., Abramson, P. D. and Spudich, J. A.** (1996). The neck region of the myosin motor domain acts as a lever arm to generate movement. *Proc. Natl. Acad. Sci. USA* **93**, 4459-4464.
- Uyeda, T. Q. and Titus, M. A.** (1997). The myosins of *Dictyostelium*. In *Dictyostelium – A Model System for Cell and Developmental Biology* (ed. Y. Maeda, K. Inouye and I. Takeuchi), pp. 43-64. Universal Academy Press, Tokyo, Japan.
- Wang, A., Liang, Y., Fridell, A., Probst, F. J., Wilcox, E. R., Touchman, J. W., Morton, C. C., Morell, R. J., Noben-Trauth, K., Camper, S. A. and Friedman, T. B.** (1998). Association of Unconventional Myosin MYO15 Mutations with Human Nonsyndromic Deafness DFNB3. *Science* **280**, 1447-1451.
- Wessels, D., Titus, M. A. and Soll, D. R.** (1996). A *Dictyostelium* myosin I plays a crucial role in regulating the frequency of pseudopods formed on the substratum. *Cell Motil. Cytoskel.* **33**, 64-79.
- Wu, C., Lee, S. F., Furmaniak-Kazmierczak, E., Côté, G. P., Thomas, D. Y. and Leberer, E.** (1996). Activation of myosin-I by members of the Ste20p protein kinase family. *J. Biol. Chem.* **271**, 31787-31790.
- Yazu, M., Adachi, H. and Sutoh, K.** (1999). Novel *Dictyostelium* unconventional myosin MyoK is a class I myosin with the longest loop-1 insert and the shortest tail. *Biochem. Biophys. Res. Comm.* **255**, 711-716.
- Yeung, A. and Evans, E.** (1989). Cortical shell-liquid core model for passive flow of liquid-like spherical cells into micropipets. *Biophys. J.* **56**, 139-149.
- Zhelev, D. V. and Hochmuth, R. M.** (1995). Mechanically stimulated cytoskeleton rearrangements and cortical contraction in human neutrophils. *Biophys. J.* **68**, 2004-2014.
- Zhelev, D. V., Needham, D. and Hochmuth, R. M.** (1994). Role of the membrane cortex in neutrophil deformation in small pipets. *Biophys. J.* **67**, 696-705.